이학석사 학위논문

# Fabrication of highly efficient surface plasmon-enhanced dye sensitized solar cells

# 표면 플라즈몬 현상을 이용한 염료감응태양전지

2012 년 8 월

서울대학교 대학원

화학부 물리화학 전공

이 혜 연

# Fabrication of highly efficient surface plasmon-enhanced dye sensitized solar cells

# 표면 플라즈몬 현상을 이용한 염료감응태양전지

지도교수 서 정 쌍

이 논문을 이학석사 학위논문으로 제출함

2012 년 8 월

서울대학교 대학원
화학부 물리화학 전공
이 혜 연

이혜연의 이학석사학위논문을 인준함
2012 년 8월

위 원 장 강 헌 (인)

부위원장 서 정 쌍 (인)

위 원 홍 종 인 (인)

# Fabrication of highly efficient surface plasmon-enhanced dye-sensitized solar cells

**By Heayeon Lee**

**Supervisor: professor Jung-Sang Suh**

**Major: Physical chemistry**

**August 2012**

**School of Chemistry**

**Graduate School**

**Seoul National University**

# ABSTRACT

## Fabrication of highly efficient surface plasmon-enhanceddye-sensitized solar cells

**By Heayeon Lee**

We have enhanced the photoconversion efficiency of surface plasmon-enhanced dye-sensitized solar cells (DSSCs) by incorporating anisotropic Ag nanoparticleswhich localized surface plasmonswere capable of enhancing theoverall visible range into conventional $TiO_2$ DSSCs. Anisotropic Ag nanoparticles with plate geometries were prepared via geometric control in the presence of citrate stabilizers, exhibiting various modes of surface plasmon resonances covering an overall visible range from 400 to 700 nm. As a result, the photocurrent density of DSSCs was increased greatly by increasing adsorption of dye molecules. The surface of anisotropic Ag nanoparticles was coated with $TiO_2$ to prevent metal corrosion and charge recombination by post-treatment of $TiO_2$/Ag nanoparticle films with titanium(IV)isoproxide.By incorporating even a small amount (0.3 wt% to that of $TiO_2$) of colloidal

anisotropic particles into $TiO_2$ DSSCs the photoconversion efficiency was improvedconsiderably from 8.0 to 9.6%.

**Keyworlds:** **s**ilver, nanoparticles, nanoplates, surface plasmon, $TiO_2$, dye-sensitized solar cell.

**Student number** : 2010-20292

# CONTENTS

# LIST OF TABLES

# LIST OF FIGURES

# CHAPTER 1. Introduction to Surface Plasmon-Enhanced Dye Sensitized Solar Cell

## 1.1 Dye-sensitized solar cell (DSSC)

Since a dye-sensitized solar cell (DSSC) based on $TiO_2$ films and ruthenium sensitizers was developed by O'Regan and Gratzel,[1–3] great attention has been devoted to the DSSCs due to high their transparency and low-cost photovoltaic performance. The DSSCs consist of conducted FTO-covered glasses, $TiO_2$ nanoparticle films, dye, and electrolytes. $TiO_2$ nanoparticle films are comprised of three parts thin blocking layer, active layer, and scattering layer. The thin blocking layer prevents back transfer of electrons to electrolytes and the active layer is working electrode. 400 nm $TiO_2$ nanoparticles are used for scattering layer which enhances light adsorption. Various photosensitive ruthenium-based dyes such as N719, N3 and blank dye are used as sensitizer(S). Electrolyte is organic solvent which contains iodide/triiodide ($3I^-/I^{3-}$) couple. The operation of principles of DSSC was shown in Figure 1.1. Photo-excited electrons from the dye inject into the conduction band of $TiO_2$ nanoparticles. The electrons of dye were regenerated by a redox system of electrolytes.

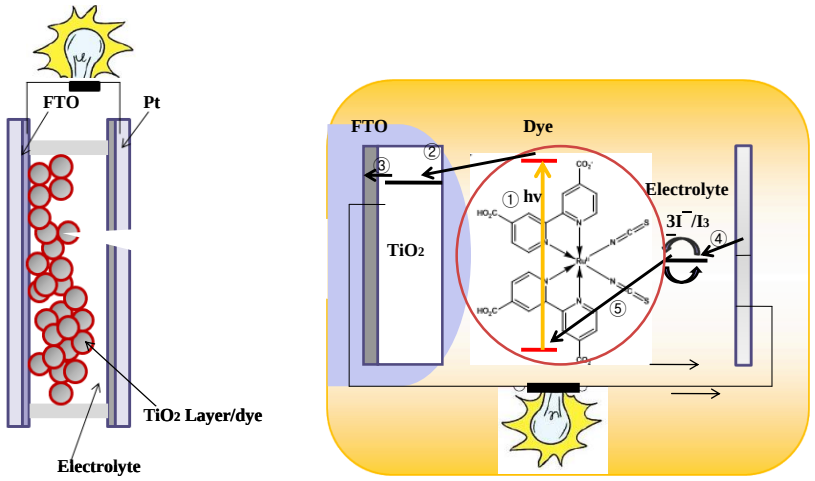


**Figure 1.1.** Schematic illustration for operation of dye-sensitized solar cell (DSSC).

Equation (1-3) explained the photoelectric chemical process of DSSC. Performance of DSSC explained via three main parameters such as short-circuit current (*Jsc*), open–circuit voltage (*Voc*), fill factor (*ff*), and The photoelectric energy conversion efficiencies (PCE). *Voc* is a difference between redox potential of electrolyte and Fermi level $TiO_2$ nanoparticles. *Jsc* is the maximum current when voltage is zero, and is dependent upon area of DSSC, number of photon, and light intensity. *ff* indicates the ratio of the maximum power to the product of *Voc* * *Jsc*. PCE is ratio of output energy from DSSC to input energy from l sun.

$$TiO_2|S + h\nu \rightarrow TiO_2|S^* \quad \textit{excitation} \quad (1)$$

$$TiO_2|S^* \rightarrow TiO_2|S^+ + e^- (CB) \quad \textit{injection} \quad (2)$$

$$TiO_2|2S^+ + 3I^- \rightarrow TiO_2|2S + I_3^- \quad \textit{regeneration} \quad (3)$$

## 1.2.Surface plasmons of silver nanoparticles

Noble metallic nanostructures composed of Au, Ag, Cu, Pd, Al, and Pt can exhibit unique colors due to strong surface plasmon resonances. Conduction electrons at the interface of noble metal and dielectric medium can be excited by incident light, and subsequently, undergo coherent oscillation, so called surface plasmons. In the case of metallic nanoparticles under resonance conditions, the motion of electrons can be confined within the nanostructured metal (*localized* surface plasmons).

In general, it has been found that the surface plasmon resonances are highly dependent upon nanoparticle size, geometry and interparticle spacing. Ag and Au nanoparticles have been of particular interest due to not only tunable plasmon resonances ranging from the visible to near-infrared regions but promising applications including sensitive biological sensing, surface-enhanced Raman scattering, plasmon-enhanced photovoltaic cells. Surface plasmon resonances are capable of inducing strong enhancement of

electromagnetic field around the surface of metallic nanoparticles. It has been widely accepted that strong surface enhancement in surface-enhanced Raman scattering is mainly contributed by the optical field enhancement generated around the surfaces of nanostructured metals. Tailoring surface plasmons is critical for the manipulation of performance in plasmonic applications using, and can be allowed by control of sizes and geometries of the nanostructured metals.

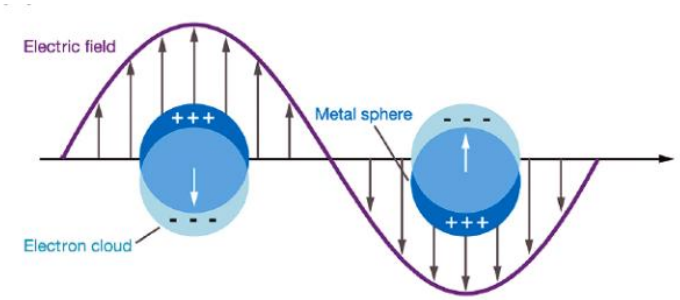


**Figure 1.2.** Schematic illustration of localized surface plasmon resonance for spherical nanoparticles. [4]

## 1.3. Photocurrent enhancement by surface plasmons in DSSC

Enhanced electromagnetic fields induced by surface plasmons have been also utilized for improving power conversion efficiency in photovoltaic cells, in particular DSSCs where ruthenium dyes have been employed as sensitizers for operating DSSCs. The absorption behavior of the dyes can be remarkably influenced by surface plasmons arising from metallic nanoparticles. It has been demonstrated in literatures that incorporation of silver nanoparticles in DSSCs caused a significant increase in the absorption of dyes located close to the nanoparticles. Although the surface coating of metallic nanoparticles with oxides for preventing metal corrosion and charge recombination at the particle surfaces by electrolytes should be required, even a small amount of the metallic particles can lead directly to remarkable photocurrent enhancement. As a result, the photoconversion efficienty of dye-sensitized photovoltaic cells can be improved by surface plasmons arising from incorporated metallic nanoparticles due to the photocurrent enhancement.

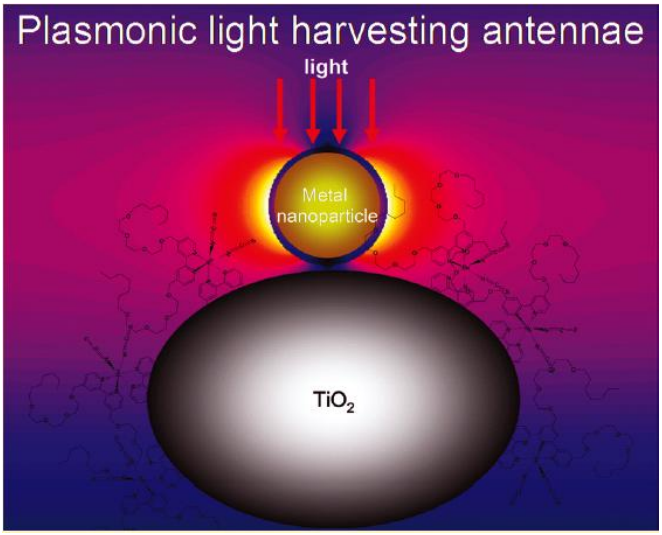


**Figure 1.3.** Schematic illustration for plasmon-enhanced light absorption of dye molecules in DSSCs.[5]

# CHAPTER 2. Surface plasmon-enhanced DSSCs incorporated with silver nanoplates

## 2.1 Introduction

Dye-sensitized solar cells (DSSCs) have received much attention because of their high power conversion efficiency and low-cost.[1-3] In the fabrication of DSSCs, mesoporous $TiO_2$ films and ruthenium sensitizers have been used as the main component materials. The power conversion efficiency of DSSCs is affected by several factors: molar absorption coefficiency, energetically suitable HOMO-LUMO levels, available surface area for dyes, transport kinetics of the electrons, regeneration by a redox couple, and losses of recombination and back reactions.[6,7] The efficiency of DSSCs will increase when the number of dye molecules adsorbed on a $TiO_2$ film increases. One could increase simply the total number of dye molecules adsorbing on $TiO_2$ film by increasing the thickness of $TiO_2$ film.[33] However, the electron transfer length to an electrode may increase with increasing the thickness of $TiO_2$ film. Therefore, the efficiency of DSSCs will not increase linearly with increasing the total number of dyes adsorbing by increasing the thickness of $TiO_2$ film. It will be very advantageous if one could increase the effective number of dye

molecules without increasing the thickness of $TiO_2$ film.

Diverse optical properties of metal nanoparticles like silver and gold are generated mainly by their localized surface plasmon.[8-11] Localized surface plasmon is excited when the frequency of light photons matches coherently the frequency of the collective oscillation of conduction electrons in metal nanoparticles. One of the most interesting features of localized surface plasmon resonance behavior is an enhanced light absorption of molecules adsorbed on noble nanoparticles like silver or gold.[12-14] The principle of localized surface plasmon has been applied to increase the optical absorption and photocurrent in a wide range of solar cell configurations.[15-22] Therefore, in order to optimize the surface plasmon effect the size and shape of nanoparticles should be controlled to match their absorption band to natural sunlight. It is known that bare metal nanoparticles are in contact directly with the dye and the electrolyte, and the recombination and back reaction of photogenerated carriers could occur.[5,15,16] Therefore, the surface of metal nanoparticles should be passivated with insulator or semiconductor. Recently, to overcome these problems, core-shell nanoparticles, in which the surface of metal nanoparticles is passivated with insulator or semiconductor such as $SiO_2$ and $TiO_2$, have been adapted.[5,15] The power conversion efficiency of DSSCs was improved significantly up to 9%. Optimum efficiency of the

DSSCs from the previous results was achieved by including small amount of silver nanoparticles with relatively small sizes (<30 nm). The light over limited spectral ranges below 500 nm can be used to excite the localized surface plasmons.[15,16] If silver nanoparticles exhibiting surface plasmon resonances extending to longer wavelength are expected to be advantageous to absorb the wider spectral range of incident light. In fabricating plasmon-enhanced DSSCs, the nanoparticles maintaining colloidal stability without aggregation should be required when transferred into $TiO_2$ nanoparticle films. Here, we have controlled the geometry of silver nanoparticles to show the localized surface plasmon resonances covering overall visible ranges. Silver nanoprticles were prepared to have plate geometries and capable of well-defined diverse modes of surface plasmon resonances such as in-plane and out-of-plane components. Also, the silver nanoplates can exhibit superior colloidal stability during phase transfer into $TiO_2$ nanoparticle films. Using the anisotropic silver nanoparticles, we could achieve the power conversion efficiency of the DSSCs based on $TiO_2$/Ag nanoparticles up to 9.6%

## 2.2 Experimental

### 2.2.1 Preparation of Ag seed clusters.

A 20 mL of aqueous solution containing 1 mM sodium citrate and 0.15 mM silver nitrate was prepared. A 2-mL aliquot of sodium borohydride (1 mM) was added into the solution under agitation. The mixture was left to react for 3 h. And then the Ag seed solution was diluted by a factor of 2 using a 1 mM sodium citrate solution.

### 2.2.2 Preparation of colloidal Ag nanoplates.

The anisotropic growth of Ag nanoplates was initiated by adding growth solutions containing the appropriate amount of silver nitrate (0.30 mM) and ascorbic acid as a reducing agent into the seed solution. The molar ratio of ascorbic acid to Ag(I) for the growth solution was fixed to be 1.5. The gradual seeded growth of Ag nanoplates progressed during 30 min. To obtain nanoplates with the average size of ~ 54 ± 4 nm in width, additional two cycles of growth processes were repeated using the growth solutions containing the same molar ratio of ascorbic acid to Ag(I).

### 2.2.3 Preparation of $TiO_2$ and Ag nanoparticle-incorporated $TiO_2$ films.

Multilayered $TiO_2$ films were used as photoanodes for DSSCs. Ti(IV) *bis*-(acetylacetonate) diisopropoxide (Aldrich, 75%) solutions were placed on fluorine-doped tin oxide (FTO) glasses by spin coating, and annealed at 450 ℃ for 1 hr to form blocking layers prior to deposition of subsequent $TiO_2$ layers. The incorporation of silver nanoparticles into $TiO_2$ photoanode was carried out for nanocrystalline $TiO_2$ layers. Controlled amounts of Ag colloids in methyl alcohol were mixed with $TiO_2$ nanoparticle pastes (HT/SP, Solaronix), and then the solvent was removed in vacuo. The ratios of [Ag] to [$TiO_2$] were adjusted from 0.07 to 0.56 wt %. A set of $TiO_2$ pastes with and without Ag nanoparticles were deposited on the FTO glass samples by doctor blading, and followed by annealing at 450 ℃ for 1 hr to form nanocrystalline $TiO_2$ layers. A $TiO_2$ paste containing 400 nm-sized particles (DSL 18NR-AO, Dyesol) was deposited to form scattering layers in similar fashion, resulting in multilayered $TiO_2$ films. The resulting films were refluxed in titanium isopropoxide (TIP) solutions (0.1 M in isopropyl alcohol) for 30 min, and followed by annealing at 450 ℃ for 30 min.

**2.2.4 Fabrication of dye-sensitized solar cells (DSSCs).**

$TiO_2$ photoanodes were immersed into ethanolic solutions of N719 (Solaronix) under heating to 50 ℃ for 12 hr. The dye-sensitized $TiO_2$ photoanodes were combined with Pt-counter electrodes. The counter electrodes were prepared by placing a drop of $H_2PtCl_6$ solutions on FTO glasses and annealed at 450 ℃ for 15 min. The composition of the electrolyte was as follows: 0.7 M 1-butyl-3-methyl-imidazolium iodide (BMII), 0.03 M $I_2$, 0.1 M guanidium thiocyanate (GSCN), and 0.5 M 4-tert-butyl pyridine (TBP) in a mixture of acetonitrile and valeronitrile (85 : 15 v/v).[31]

## 2.3 Results and Discussion

### 2.3.1. Anisotropic growth of colloidal Ag nanoplates.

Ag seeds were prepared via the rapid reduction of Ag(I) by sodium borohydride. Trisodium citrate was employed as an ionic stabilizer to obtain small spherical Ag clusters with the sizes ranging from 7 to 12 nm. Anisotropic growth of Ag nanoplate was allowed using ascorbic acid via gradual reduction processes in the presence of seeds. After three cycles of growth processes, the colloids containing plate geometries were obtained in the prescence of citrate without any additional stabilizers. Figure 2.1 shows transmittance electron microscopy (TEM) images of Ag nanoparticles after each cycle of anisotropic growth processes. The width of Ag nanoparticles was gradually increased, repeating growth processes. After three cycles of growth processes which incorporated DSSC the predominant geometries of typical Ag colloids were revealed to be hexagonal plates with the average width of ~54 ± 4 nm by transmittance electron microscopy. A minor proportion of spherical particles were also observed up to about 26% in the whole colloid.

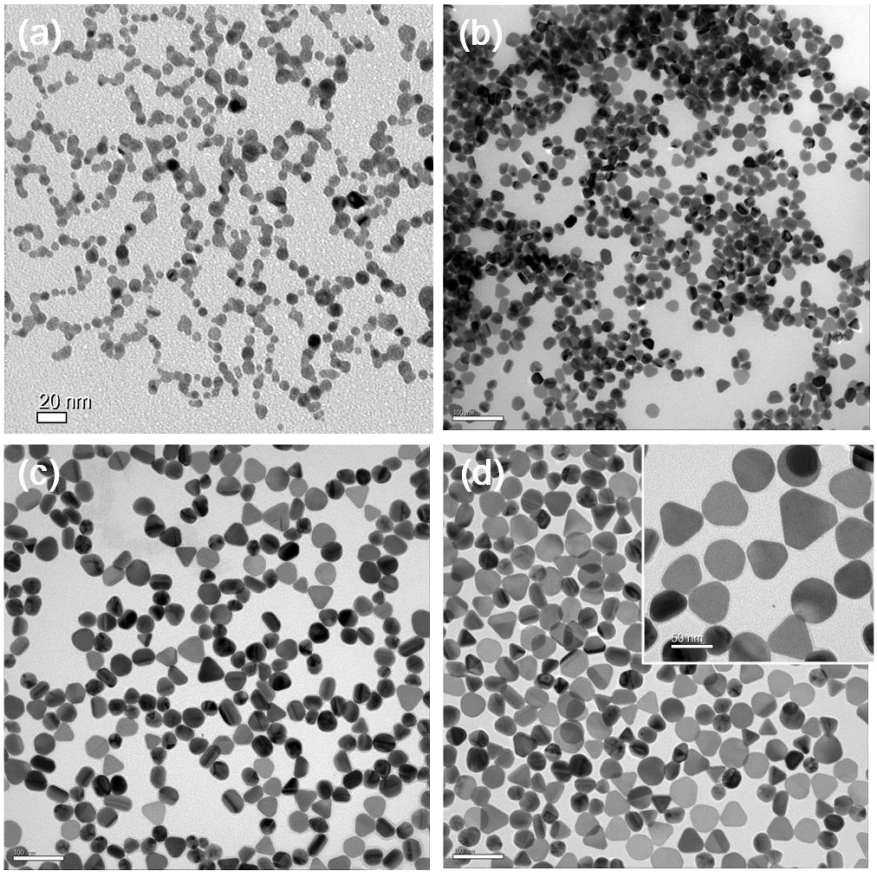


**Figure 2.1.** TEM images taken at each processing stage. (a) Ag seeds, (b) first cycle (c) second cycle, (d) third cycle, an insert shows a magnified view of Ag nanoplates.

In Figure 2.2, the photograph shows the different colors orginated from surface plasmon resonances of Ag colloids after different cycles of particle growth. The Ag colloid prepared after the first growth process displays orange yellow, and the color turned orange by repeating growth process. Finally, a colloid exhibiting pale red was obtained after three cycles of growth processes.

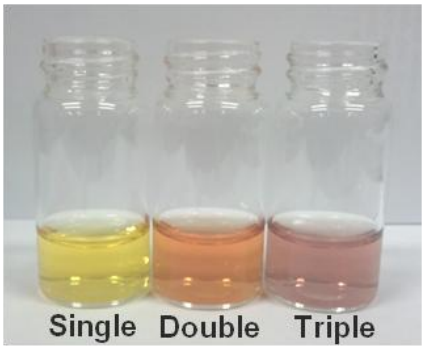


**Figure 2.2.** A photograph image displaying different colors of Ag colloids after anisotropic growth processes.

Extinction spectra corresponding to colloidal Ag seeds and nanoparticles were depicted in Figure 2.3. The seed colloids displayed a surface plasmon resonance (SPR) peak with the maximum wavelength ($\lambda_{max}$) at 390 nm. The red-shift of extinction spectra was observed after each cycle and in-plane dipole plasmon resonances gradually emerged at the second cycle. A remarkable change in the extinction profile was observed at third cycle which formed hexagonal nanoplates. An extinction spectrum measured from nanoplates shows double-peaked plasmon resonances, which extended to the red region. The $\lambda_{max}$ of two strong peaks were measured to be 426 and 554 nm, respectively. The SPR peak located at longer wavelength (~550 nm) is originated from in-plane dipolar plasmon resonances of hexagonal plates, while another one may be attributed to out-of-plane dipolar plasmon resonances. The contribution of nanospheres to the extinction of silver colloids cannot be excluded. The nanospheres with the size below 50 nm also showed similar spectral ranges compared to the out-of-plane plasmon resonances of plates. A weak peak observed at around 335 nm can be assigned to the quandrupolar plasmon resonances.

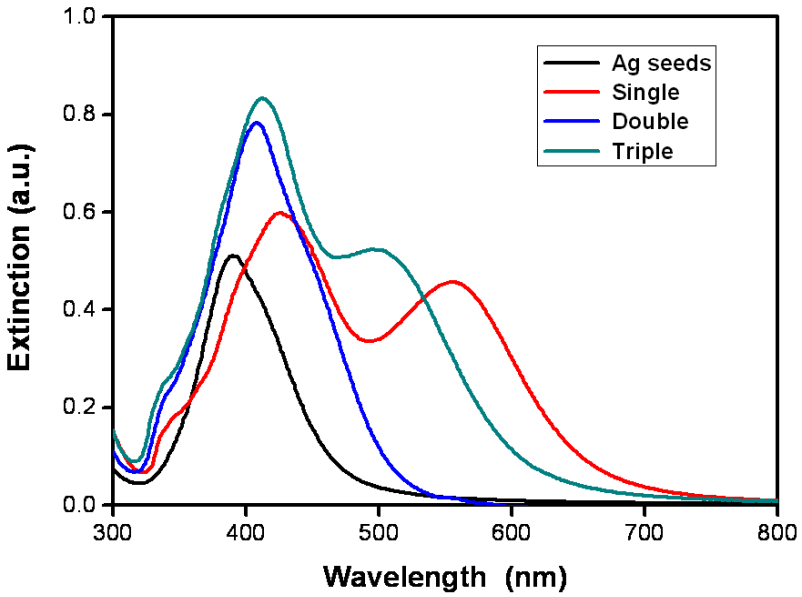


**Figure 2.3.** Extinction spectra measured from Ag seeds and anisotropic Ag colloids after reduction processes.

### 2.3.2 Surface plamon-enhanced DSSCs incorporated with silver nanoplates.

Two different types of DSSCs were fabricated to investigate the effect of surface plasmons from silver nanoplates on photovoltaic parameters of DSSCs. One is conventional $TiO_2$-based DSSCs ($TiO_2$ only), and the other is plasmon-enhanced DSSCs via incorporation of anisotropic Ag nanoparticles in the $TiO_2$ DSSCs. In the case of DSSCs incorporated with Ag nanoparticles, post-treatment with titanium isopropoxide ($TiO_2$/Ag─TIP) was required to prevent the direct corrosion of Ag nanoparticle and photogenerated charge recombination by electrolytes. Figure 2.4 shows photocurrent density-voltage (*J*-*V*) curves of $TiO_2$-only DSSCs, and $TiO_2$/Ag-TIP DSSCs were measured under 1 sun. Photovoltaic parameters were shown in Table 2.1. Under the optimum condition where the 0.3 wt % of Ag nanoparticles, the photoelectric energy conversion efficiencies (PCE) of $TiO_2$-only, and TiO2/Ag-TIP DSSCs were 8.00 % , and 9.56 %, respectively. PCE was increased 20% by enhancing short-circuit current ($J_{sc}$). Open-circuit-voltage ($V_{oc}$) and fill factor (*ff*) were close both $TiO_2$-only and Ag NP-$TiO_2$, while photocurrent density was increased significantly from 13.85 mA/cm$^2$ to 16.46 mA/cm$^2$ by localized surface plasmon effect of Ag nanoplates.

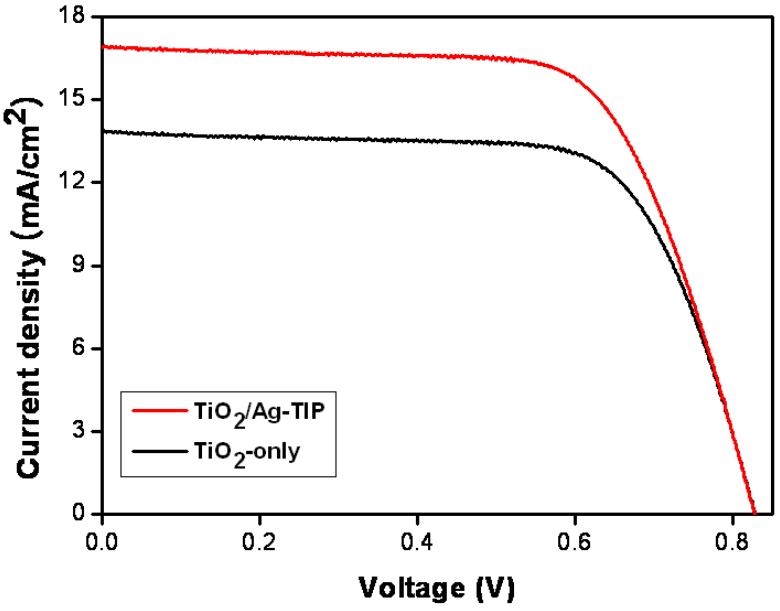


**Figure 2.4.** Photocurrent density-applied voltage characteristics of $TiO_2$-only and $TiO_2$/Ag-TIP DSSCs.

| | $J_{sc}$ (mA/cm$^2$) | $V_{oc}$ (V) | *Ff* | $\eta$ (%) |
|---|---|---|---|---|
| **(a)** | **13.85** | **0.83** | **0.70** | **8.00** |
| **(b)** | **16.46** | **0.84** | **0.70** | **9.56** |

**Table 2.1.** Photovoltaic parameters of DSSCs without and with Ag nanoplates.

To clarify the effect of surface plasmons arising from the Ag nanoparticles on the absorption of dye, optical spectra of two different $TiO_2$ films with and without Ag nanoparticles were systematically monitored. Figure 2.5 (Top) was indicated extinction spectra recorded from $TiO_2$-only and $TiO_2$/Ag-TIP films before dye adsorption. $TiO_2$ has a large band gap of 3.2 eV, which corresponds to UV region below 400 nm. Compare to $TiO_2$-only film, the adsorption of $TiO_2$/Ag-TIP film was increased.

Vivid absorption bands at about 390 and 530 nm in the visible range emerged after dye adsorption on the two different films due to the metal-to-ligand charge transfer transitions of ruthenium dye molecules.[32] A significant difference in the absorption intensity of dyes was, however, found between $TiO_2$-only and Ag nanoparticle-incorporated $TiO_2$ films. As shown in figure 2.5 (bottom), the absorption of dyes was increased by a factor of 1.23 by incorporating even a small amount of Ag nanoaparticles (0.3 wt %) into $TiO_2$ films. The dye adsorption was increased by excitation of localized surface Plasmon (LSP) of Ag nanoplates. The peak position of dye adsorption was slightly blue-shifted in the present of Ag nanoplates on $TiO_2$ films.[15] Enhanced electromagnetic field was created when LSP occurred around Ag nanoplates by incident light. As reported previously in literature, the enhanced electromagnetic field leaded to the increase of dye adsorption due to

interaction between the dye molecular dipole and electromagnetic field of Ag nanoplates.[13-16]

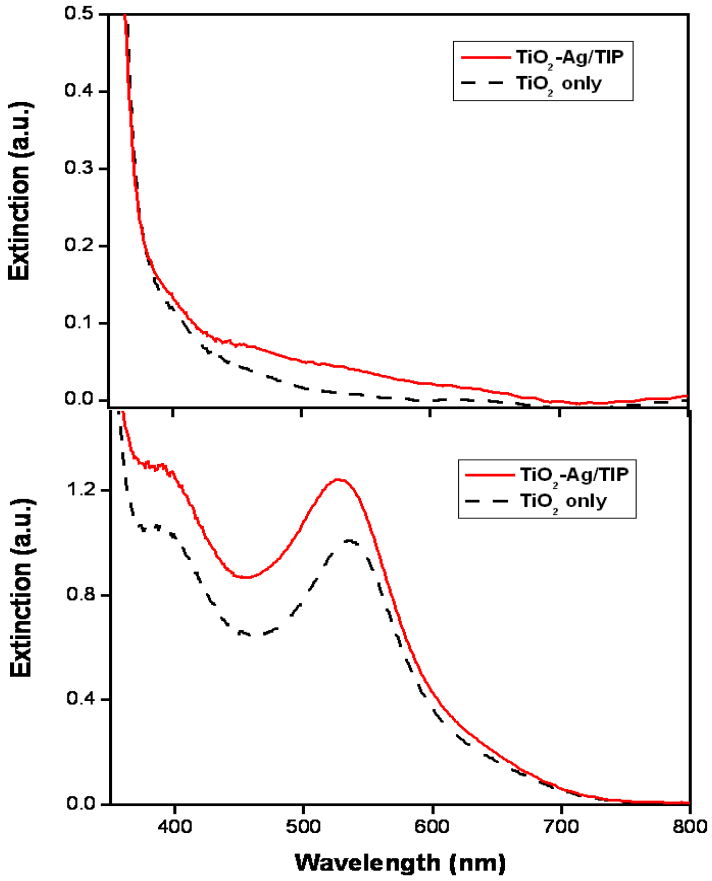


**Figure 2.5.** UV-visible spectra of $TiO_2$-only (dashed) and $TiO_2$/Ag-TIP (solid) films. (Top) before N719 dye adsorption, (Bottom) after N719 dye adsorption.

Incident photon-to-current efficiency (IPCE) was measured from DSSCs with and without Ag nanoplates (Figure 2.6). The IPCE indicated light harvesting, charge collection, and charge injection efficiencies.[15] The IPCE over the wavelength range from 400 to 700 nm was enhanced, and the result is in consistent with the efficiency results. IPCE curves exhibit the maximum wavelength of 530 nm, which is closely associated with ruthenium dye absorption. Light harvesting increased with increasing light adsorption of dye molecule. The IPCE of Ag NP-$TiO_2$ DSSC was higher than $TiO_2$-only DSSC and the integrated IPCE value from DSSCs incorporated by Ag NPs (0.3 wt %) is higher than that from DSSCs with the lack of Ag NPs by a factor of 1.21, which is found to be close to the relative ratio (~1.19) of $J_{sc}$ values taken from a comparison between $TiO_2$ only and $TiO_2$/Ag-TIP DSSCs with the optimum concentration of Ag nanoparticles.

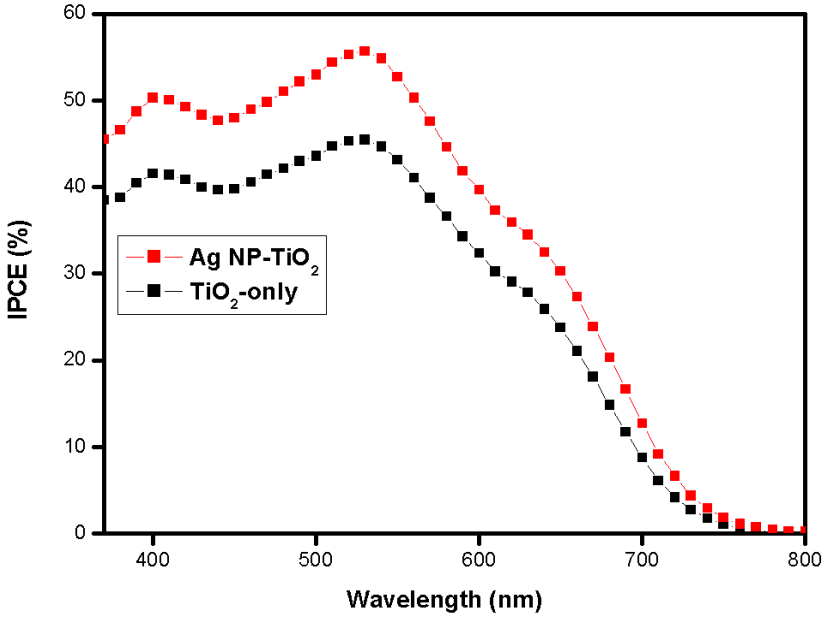


**Figure 2.6.** IPCE spectra taken from $TiO_2$-only and $TiO_2$/Ag-TIP DSSCs.

The dependence of Ag nanoparticles concentration on PCE and $J_{sc}$ of plasmon-enhanced DSSCs was investigated. As shown in Figure 2.7, as the concentration of Ag nanoparticles was raised from 0.07 up to 0.30 wt %, the PCE was gradually increased from 8.9% up to the maximum value. A further increase in the concentration of Ag nanoparticles to 0.60% rather causes the decrease in the PCE values to 7.9%. A trend observed from the change in PCE values was found to be in good agreement with that from a change in photocurrent density. *Jsc* values were enhanced from 15.91 to 16.41 mA/cm$^2$ as the concentration of Ag nanoparticles approached 0.30 wt %, and a further increase of Ag concentration led to a decrease in $J_{sc}$. Increased trapping of photogenerated electrons by too high concentrations of Ag nanoparticles may result in the relative decrease in the photocurrent density and eventually, the PCE of plasmon-enhanced DSSCs.

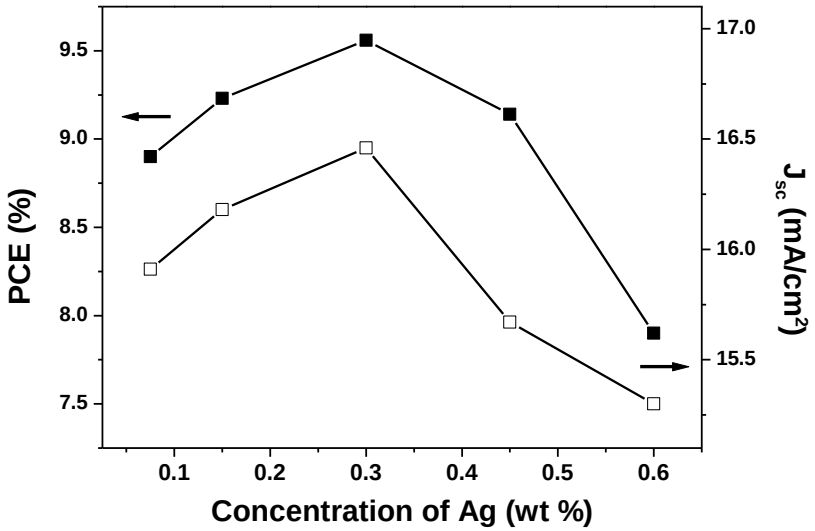


**Figure 2.7.** Dependence of Ag nanoparticle concentrations on PCE and $J_{sc}$ values.

## 2.4. Conclusions

Surface plasmon-enhanced DSSCs were fabricated by incorporating silver nanoparticles in $TiO_2$ nanoparticle films. The colloidal silver nanoaprticles were synthesized via anisotropic growth in the presence of preformed seeds. The broad extinction was observed from silver nanoparticles, exhibing the diverse modes of surface plasmon resonances due to plate geometries. Monitoring photovoltaic parameters, we confirmed that the photocurrent density was significantly enhanced, giving rise to an increase in the photoconversion efficiency of plasmon enhanced DSSCs by up to 20% compared to conventional $TiO_2$ DSSCs. In addition, the absorption of dye molecules adsorbed on $TiO_2$ nanoaprticle films with and without including anisotropic silver nanoparticles was investigated. The strong enhancement in dye adsorption was observed from DSSCs incorporated with even a relatively small amount of silver NPs (0.3 wt % relative to weigh of $TiO_2$). We believed that surface plasmons of anisotropic silver nanoparticles contribute mainly to the increased dye absorption, which can result in strong photocurrent enhancement. From plasmon-enhanced DSSCs incorporated with anisotropic Ag nanoparticles, the power conversion efficiency was confirmed to be improved from 8.0 to 9.6%.

## REFERENCES


1. Oregan, B.; Gratzel, M. *Nature* **1991**, *353*, 737-740.

2. Gratzel, M. *Inorganic Chemistry* **2005**, *44*, 6841-6851.

3. Kim, Y. J.; Lee, M. H.; Kim, H. J.; Lim, G.; Choi, Y. S.; Park, N. G.; Kim, K.; Lee, W. I. *Adv. Mater.* **2009**, *21*, 3668.

4. Willets, K. A.; Van Duyne, R. P., Annual Review of Physical Chemistry 2007 , 58 , 267-297

5. Brown, M. D.; Suteewong, T.; Kumar, R. S. S.; D'Innocenzo, V.; Petrozza, A.; Lee, M. M.; Wiesner, U.; Snaith, H. J. *Nano Letters* **2011**, *11*, 438-445.

6. Ghicov, A.; Albu, S. P.; Hahn, R.; Kim, D.; Stergiopoulos, T.; Kunze, J.; Schiller, C. A.; Falaras, P.; Schmuki, P. *Chemistry-an Asian Journal* **2009**, *4*, 520-525.

7. Wang, Z. S.; Kawauchi, H.; Kashima, T.; Arakawa, H. *Coordination Chemistry Reviews* **2004**, *248*, 1381-1389.

8. Haynes, C. L.; Van Duyne, R. P. J. Phys. Chem. B 2001, 105, 5599

9. Michaels, A. M.; Mirmal, M.; Brus, L. E. J. Am. Chem. Soc. 1999, 121, 9932.

10. Kelly, K. L.; Coronado, E.; Zhao, L. L.; Schatz, G. C. J. Phys. Chem. B 2003, 107, 668.

11. Link, S.; El-sayed, M. A. J. Phys. Chem. B 1999, 103,8410.

12. Ihara, M.; Tanaka, K.; Sakaki, K.; Honma, I.; Yamada, K. *Journal of Physical Chemistry B* **1997,** *101* (26), 5153-5157.

13. Standridge, S. D.; Schatz, G. C.; Hupp, J. T. *Langmuir* **2009,** *25* (5), 2596-2600.

14. Standridge, S. D.; Schatz, G. C.; Hupp, J. T., *J. Am. Chem. Soc.* **2009,** *131* (24), 8407-8409.

15. Jeong, N. C.; Prasittichai, C.; Hupp, J. T. *Langmuir* **2011,** *27* (23), 14609-14614.

16. Qi, J. F.; Dang, X. N.; Hammond, P. T.; Belcher, A. M. *Acs Nano* **2011,** *5* (9), 7108-7116

17. Ishikawa, K.; Wen, C. J.; Yamada, K.; Okubo, T. *J. Chem. Eng. Jpn*. **2004**, *37*, 645

18. Wu, J.-L.; Chen, F.-C.; Hsiao, Y.-S.; Chien, F.-C.; Chen, P.; Kuo, C.-H.; Huang, M. H.; Hsu, C.-S. *ACS Nano* **2011**, *5*, 959.

19. Westphalen, M.; Kreibig, U.; Rostalski, J.; Lüth, H.; Meissner, D. *Sol. Energy Mater. Sol. Cells* **2000**, *61*, 97.

20. Rand, B. P.; Peumans, P.; Forrest, S. R. *J. Appl. Phys*. **2004**, *96*, 7519.

21. Morfa, A. J.; Rowlen, K. L.; Reilly, T. H.; Iii; Romero, M. J.; van de Lagemaat, J. *Appl. Phys. Lett*. **2008**, *92*, 013504.

22. Konda, R. B.; Mundle, R.; Mustafa, H.; Bamiduro, O.; Pradhan, A. K.; Roy, U. N.; Cui, Y.; Burger, A. *Appl. Phys. Lett*. **2007**, *91*, 191111.

23. Stuart, H. R.; Hall, D. G. *Appl. Phys. Lett*. **1998**, *73*, 3815.

24. Schaadt, D. M.; Feng, B.; Yu, E. T. *Appl. Phys. Lett*. **2005**, *86*, 063106.

25. Derkacs, D.; Lim, S. H.; Matheu, P.; Mar, W.; Yu, E. T. *Appl. Phys. Lett*. **2006**, *89*, 093103.

26 Pillai, S.; Catchpole, K. R.; Trupke, T.; Green, M. A. *J. Appl. Phys*. **2007**, *101*, 093105.

27. Hagglund, C.; Zach, M.; Kasemo, B. *Appl. Phys. Lett*. **2008**, *92*, 013113.

28. Zhao, G.; Kozuka, H.; Yoko, T. *Sol. Energy Mater. Sol. Cells* **1997**, *46*, 219.

29. Wen, C.; Ishikawa, K.; Kishima, M.; Yamada, K. *Sol. Energy Mater. Sol. Cells* **2000**, *61*, 339.

30. Ding, I. K.; Zhu, J.; Cai, W.; Moon, S.-J.; Cai, N.; Wang, P.; Zakeeruddin, S. M.; Grätzel, M.; Brongersma, M. L.; Cui, Y.; et al. *Adv. Energy Mater*. **2011**, *1*, 51.

31. Park, N. G. *Journal of Chemical Engineering* **2010,** *27* (2), 375-384.

32. Farah Matar.; Tarek H. Ghaddar.; Kate Walley.; Tracy DosSantos.; James R.; Durrant.; Brian O'Regan J. Mater. Chem., **2008**, 18, 4246–4253

33. Man Gu Kang.; Kwang Sun Ryu.; Soon Ho Chang.; Nam Gyu Park.; Jin Sup Hong.; Kang-Jin Kim.; *Bull. Korean Chem. Soc*. **2004**, Vol. 25, No. 5

## APPENDIX/ Plasmon-enhanced DSSCs incorporated with silver nanospheres.

**Seeded growth of spherical silver nanoparticles.** To obtain monodisperse and spherical silver nanoparticles were prepared via a two-step chemical reduction process. In the presence of preformed silver nanoclusters as seeds (see **Chapter 2**) the gradual growth into nanoparticles was conducted. Aqueous Ag(I) was reduced rapidly by sodium borohydride as a strong reducing agent. Trisodium citrate acting as an ionic stabilizer has an important role in the formation of small size spherical clusters, preventing coalescence of Ag nuclei by the rapid reduction rate. By adding the seeds in the growth solutions containing additional amounts of Ag(I) and ascorbic acid, seeded growth of spherical silver nanoparticles progressed gradually due to the relatively slow reduction rate adjusted by ascorbic acid. Figure 1 shows monodisperse spherical silver nanoparticles with the average size of 27 nm were obtained via seeded growth. A strong localized surface plasmon resonance was observed. A single dipolar peak emerged, exhibiting $\lambda_{max}$ at 414 nm as shown in Figure 2.

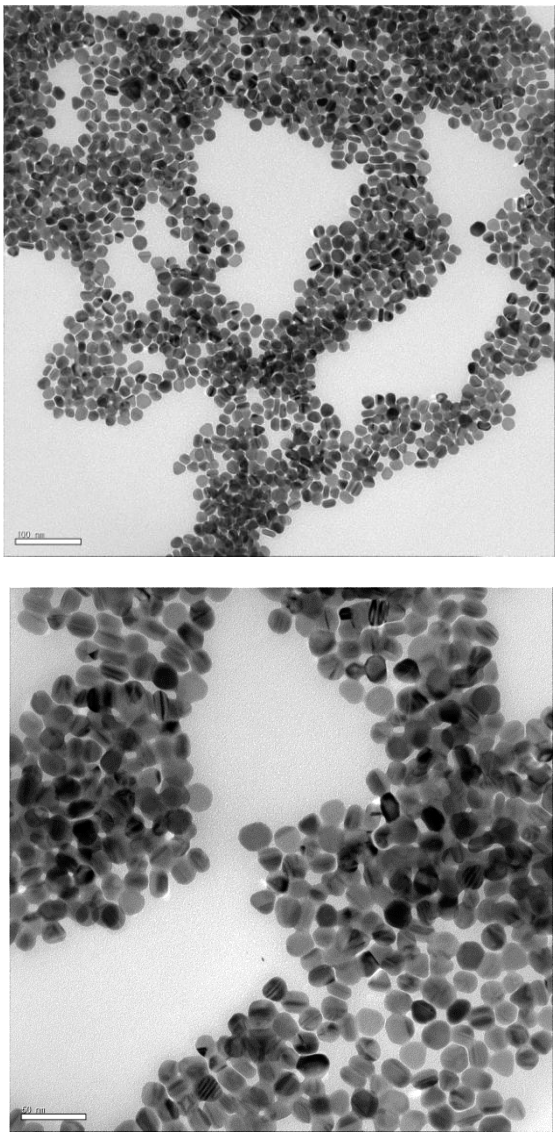

**Figure 1.** TEM images showing spherical Ag nanoparticles after seeded growth.

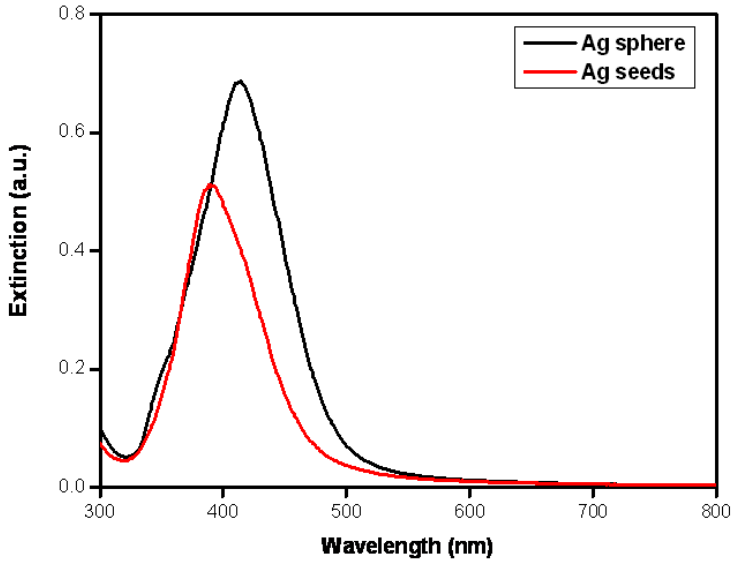


**Figure 2.** Extinction spectra of Ag seeds and nanospheres.

**Silver nanosphere-incorporated DSSCs.** Two different types of DSSCs were fabricated to investigate the effect of surface plasmons from spherical silver nanoparticles on photovoltaic parameters of DSSCs. Plasmon-enhanced DSSCs via incorporation of Ag nanospheres in the $TiO_2$ DSSCs. In the case of DSSCs incorporated with Ag nanospheres, post-treatment with titanium choloride ($TiO_2$/Ag─$TICl_4$) was required to prevent the direct corrosion of Ag nanospheres and photogenerated charge recombination by electrolytes. Figure 3 shows photocurrent density-voltage (*J-V*) curves of $TiO_2$-only DSSCs and $TiO_2$/Ag-$TICl_4$ DSSCs were measured under 1 sun. Photovoltaic parameters were shown in Table 2.1. Under the optimum condition where the 0.3 wt % of Ag nanospheres, the photoelectric energy conversion efficiencies (PCE) of $TiO_2$-only and $TiO_2$/Ag-$TICl_4$ DSSCs were 8.00 % and 9.00 %, respectively. PCE was increased 12.5 % by enhancing short-circuit current ($J_{sc}$). Open-circuit-voltage ($V_{oc}$) and fill factor (*ff*) were close both $TiO_2$-only and $TiO_2$/Ag─$TICl_4$ , while photocurrent density was increased significantly from 13.85 mA/cm$^2$ to 15.68 mA/cm$^2$ by localized surface plasmon effect of Ag nanospheres.

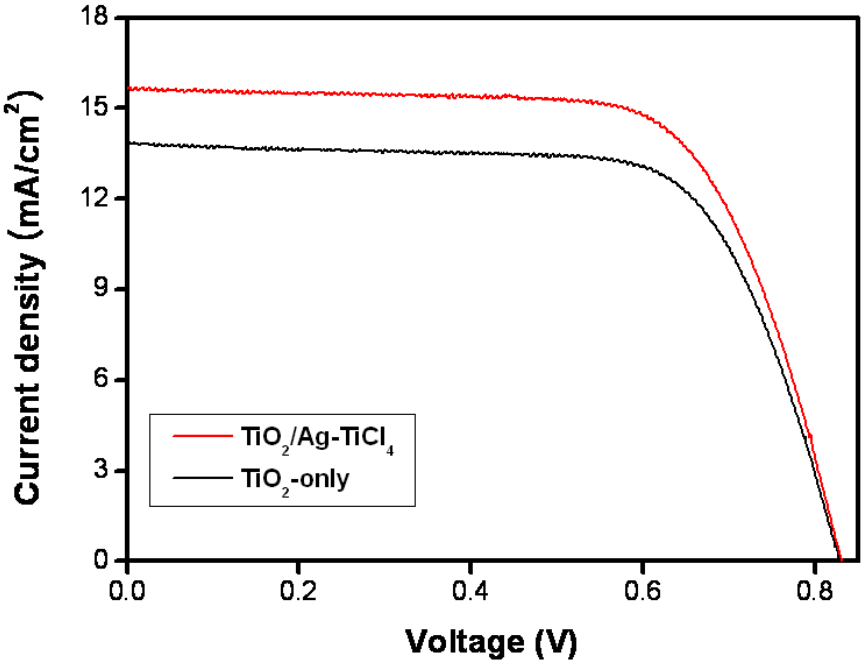


**Figure 3.** Photocurrent density-voltage curves taken from two different cells.

| | $J_{sc}$ (mA/cm$^2$) | $V_{oc}$ (V) | *ff* | *H* (%) |
|---|---|---|---|---|
| **$TiO_2$** | **13.85** | **0.83** | **0.70** | **8.00 %** |
| **$TiO_2$/Ag-$TiCl_4$** | **15.68** | **0.83** | **0.69** | **9.00 %** |

**Figure 4.** Photovoltaic parameters of two different cells.

**Conclusions.** We have investigated surface plasmon enhanced DSSCs by silver nanospheres. The colloidal silver nanspheres were synthesized via seeded growth of and spherical geometries were obtained by adding the growth solutions containing additional amounts of Ag(I) and ascorbic acid. A single extinction peak of spherical silver nanospheres was observed at 413 nm. We monitored photovoltaic parameters when the silver nanospheres incorporated DSSCs. Power conversion efficiency was increased about 12.5 % by enhancing photocurrent efficiency (*Jsc*). *Jsc* significantly enhanced from 13.85 mA/cm$^2$ to 15.68 mA/cm$^2$ by localized surface Plasmon effect of Ag nanospheres while open-circuit-voltage (*Voc*) and fill factor (*ff*) were close. As a result, the power conversion efficiency was improved from 8.0 to 9.0% by incorporating Ag nanoparticles.

## 국문 초록

### 표면 플라즈몬 현상을 이용한 염료감응태양전지

넓은 가시광선 영역에서 표면 플라즈몬 공명을 일으키는 은 나노입자를 합성한 후 염료감응형 태양전지에 도입하여 효율을 증가시켰다. 태양빛의 스펙트럼은 280 ~ 4000 nm 까지 분포 되어있으나 대부분의 에너지는 가시광선 영역인 380 ~ 780 nm 에 몰려 있다. 이 가시광선 영역의 빛을 모두 이용하고자 400 nm 부터700 nm 까지 전 가시광선 영역에 걸쳐 표면 플라즈몬 공명을 일으키는 판 형상을 가지는 은 나노입자를 합성하였다.

은 나노입자는 trisodium citrate 를 안정제로 사용하면서 Ag(I) 를 sodium borohydride (환원제) 로 빠르게 환원시켜 형성시킨 7 ~ 14 nm 크기의 은 집합체 씨앗으로 하여 성장시켰다. 이 은 씨앗에 Ag(I) 와 환원제인 ascorbic acid 를 추가적으로 첨가하여 총 3번의 반복성장과정을 통해 ~ 54 ± 4 nm 크기의 판 형상의 입자를 합성하였다. 이와 같이 합성한 은 나노입자를 염료감응형 태양전지에 도입하기 위해서는 은 나노입자가 태양전지 제작 시 사용

되는 전해질의 구성요소인 iodine에 의해 부식되는 것을 방지하여야 한다. 이를 방지하고자 은 나노입자 도입 후 titanium(IV) isopropoxide 처리를 통해 은 나노입자 표면을 $TiO_2$ 로 코팅하였다.

판 형상의 은 나노입자를 염료감응형 태양전지에 도입하여 효율을 측정해 본 결과 도입하지 않은 태양전지의 효율은 8.0 %, 은 나노입자를 도입한 태양전지는 9.6 % 로 약 20 % 정도 효율을 향상시켰다. 이러한 효율 향상은 빛이 조사되면서 은 나노입자 표면에서 나타나는 플라즈몬 공명에 의해 입자 주변의 염료 분자들의 광흡수 증가에 의해 나타난 것으로 확인 되었다. 염료 분자의 광흡수 증가로 인해 광전류 값이 13.85 $mA/cm^2$ 에서 16.46 $mA/cm^2$ 으로 20 % 가량 증가하는 것을 확인하였다.

은 나노입자의 형상을 더 정밀하게 제어하여 더 넓은 영역의 태양 빛을 이용한다면 염료감응형 태양전지의 효율을 더 증가시킬 수 있을 것이다.

**주 요 어 :** 은, 나노입자, 나노 판, 표면 플라즈몬, $TiO_2$, 염료감응형 태양전지.

**학번** : 2010-20292